HHS Public Access

Author manuscript

Biofabrication. Author manuscript; available in PMC 2018 November 14.

Published in final edited form as:

Biofabrication. ; 9(4): 044106. doi:10.1088/1758-5090/aa8fb8.

Effect of scaffold morphology and cell co-culture on tenogenic differentiation of HADMSC on centrifugal melt electrospun poly (L-lactic acid) fibrous meshes

Shaohua Wu[1,2,#], **Hao Peng**[3,#], **Xiuhong Li**[3], **Philipp N. Streubel**[4], **Yong Liu**[3,*], and **Bin Duan**[1,2,5,*]

[1]Mary & Dick Holland Regenerative Medicine Program, University of Nebraska Medical Center, Omaha, NE, USA

[2]Division of Cardiology, Department of Internal Medicine, University of Nebraska Medical Center, Omaha, NE, USA

[3]College of Mechanical and Electric Engineering, Beijing University of Chemical Technology, Beijing 100029, China

[4]Department of Orthopedic Surgery and Rehabilitation, University of Nebraska Medical Center, Omaha, NE, USA

[5]Department of Surgery, College of Medicine, University of Nebraska Medical Center, Omaha, NE, USA

Abstract

Engineered tendon grafts offer a promising alternative for grafting during the reconstruction of complex tendon tears. The tissue engineered tendon substitutes have the advantage of increased biosafety and the option to customize their biochemical and biophysical properties to promote tendon regeneration. In this study, we developed a novel centrifugal melt electrospinning (CME) technique, with the goal of optimizing the fabrication parameters to generate fibrous scaffolds for tendon tissue engineering. The effects of CME processing parameters, including rotational speed, voltage, and temperature, on fiber properties (i.e. orientation, mean diameter, and productivity) were systematically investigated. By using this solvent-free and environmentally-friendly method, we fabricated both random and aligned poly (L-lactic acid) (PLLA) fibrous scaffolds with controllable mesh thickness. We also investigated and compared their morphology, surface hydrophilicity, and mechanical properties. We seeded human adipose derived mesenchymal stem cells (HADMSC) on various PLLA fibrous scaffolds and conditioned the constructs in tenogenic differentiation medium (TDM) for up to 21 days, to investigate the effects of fiber alignment and scaffold thickness on cell behavior. Aligned fibrous scaffolds induced cell elongation and orientation through a contact guidance phenomenon and promoted HADMSC proliferation and differentiation towards tenocytes. At the early stage, thinner scaffolds were beneficial for

[*]Corresponding author: Dr. Yong Liu, yongsd@iccas.ac.cn; Phone: +86-135-2100-8075, Dr. Bin Duan, bin.duan@unmc.edu; Phone: +1-(402) 559-9637.

[#]these authors contributed equally to this study.

The authors declare no competing financial interest.

HADMSC proliferation, but the scaffold thickness had no significant effects on cell proliferation for longer-term cell culture. We further co-seeded HADMSC and human umbilical vein endothelial cells (HUVEC) on aligned PLLA fibrous mats and determined how the vascularization affected HADMSC tenogenesis. We found that co-cultured HADMSC-HUVEC expressed more tendon related markers on the aligned fibrous scaffold. The co-culture systems promoted in vitro HADMSC differentiation towards tenocytes. These aligned fibrous scaffolds fabricated by CME technique could potentially be utilized to repair and regenerate tendon defects and injuries with cell co-culture and controlled vascularization.

Keywords

fiber alignment; mesh thickness; vascularization; tendon tissue engineering; human adipose derived stem cells; human umbilical vein endothelial cells

1. Introduction

Tendon grafts are essential for the treatment of various tendon-related conditions. More than 30 million human tendon grafting procedures are performed annually worldwide [1]. Autografts, allografts, and xenografts are currently the most commonly used tendon substitutes for tendon reconstruction [2]. However, the limited availability of appropriate tendon tissues, that closely mimic the size, shape, and physiological characteristics, as well as donor site morbidity, inflammatory response, and potential disease transmission limit their clinical application [3].

Tissue engineering techniques have the potential to facilitate tendon formation and regeneration and will eventually develop functional substitutes to replace injured tendon tissues. Significant progress has been made by introducing innovative bio-scaffolds, stem cells, biological growth factors, and co-culture techniques in engineered tendon tissues [4, 5]. However, major challenges remain, and further improvements are still needed. One important aspect for tendon tissue engineering is the design of fibrous tissue scaffolds that can control the scaffold morphology and properties that mimic native tendon extracellular matrix (ECM). This can further regulate 3D cell behavior and stimulate tenocyte formation with subsequent remodeling of the ECM. Traditional strategies used for achieving fibrous scaffolds are through the utilization of dry spinning and wet spinning, in combination with weaving, knitting, braiding, or even non-weaving technology [6–9]. However, these scaffolds were usually generated from fibers with diameters larger than 10 μm, which are too large when compared to native ECM fiber dimensions, resulting in reduced cell attachment and proliferation [10].

Electrospinning has gained tremendous interest as a method for fabricating micro- or nano-fibrous biomaterial scaffolds over the past decade [11, 12]. This technique can produce fibers with diameters two to three orders of magnitude smaller than those formed by traditional processes [13, 14]. Many studies have demonstrated that electrospun fibrous scaffolds have excellent fiber size control and a high surface-to-volume ratio, which can promote cell adhesion, proliferation, and differentiation in tendon tissue engineering applications [15–18]. Moreover, some groups employed several modified electrospinning

methods to generate nanofibrous scaffolds in the novel forms, including fiber bundles [19], filament yarns [20], micro-crimped fibers [21], drug-loaded fibers [22], and nanotextured composite fibers [23], to better mimic the structure of native tendon ECM and to promote the tendon-like tissue regeneration. Nevertheless, the excess solvent in fibers fabricated by solvent-based electrospinning methods may be problematic, since the toxic inner solvent may disperse out of the fiber and damage cells and tissue [24, 25]. Although post-fabrication and treatment of electrospun samples via vacuum and heating facilitate the solvent removal process and limit toxicity [14, 26], a modified system that can exclude the solvent will still be beneficial for the in vitro and in vivo applications. Moreover, for traditional electrospinning, the tightly packed architecture limits the pore size between fibers, and poor controllability may halt cell infiltration into the inner layer of the scaffolds, further preventing the formation of 3D tissue grafts [10]. Many modified methods were developed to improve the pore size and pore structure of electrospun nanofiber meshes [14, 27]. There is still a need to develop other controllable fiber fabrication techniques to eliminate solvents and to improve controllability [28–30].

Another important aspect needed for tendon tissue engineering is improving the vascularization of engineered tendon tissues in the early stage of tendon formation and healing. Although tendon is recognized as a poorly vascularized tissue type, it generally possesses more vessels than commonly believed [31]. A rich capillary network is found in human embryonic tendon, although both cellularity and vessel density decrease in matured human tendon [32]. Moreover, there is a high expression of the proangiogenic protein, vascular endothelial growth factor (VEGF), in cells from fetal and injured human tendons, but low VEGF expression in healthy adult tendons [33, 34]. Increasing evidence has shown that higher vascularization within engineered tendon grafts plays an important role in the early tenocyte formation and host integration phase, thus promoting the healing of tendon damage or rupture [35–37].

To overcome the aforementioned challenges, a novel centrifugal melt electrospinning (CME) technique was developed by combining centrifugal spinning with melt electrospinning. Our CME can fabricate environmentally-friendly and solvent-free micro/nanofiber meshes for mimicking native tendon ECM structure. The effects of different parameters on the properties of fibrous meshes were systematically studied. We first investigated how the fiber alignment and scaffold thickness of fabricated fibrous scaffolds affected morphology, orientation, proliferation, and differentiation of human adipose derived mesenchymal stem cells (HADMSC). Then human umbilical vein endothelial cell (HUVEC) and HADMSC were further co-seeded and co-cultured in hybrid media on PLLA-aligned fibrous scaffolds to assess the effects of vascularization on HADMSC tenogenic differentiation.

2. Methods

2.1 CME equipment and fabrication of micro/nanofiber meshes

A total CME system was assembled to facilitate the large-scale production of fibrous meshes with fiber diameters ranging from nano-scale to micro-scale in Fig. 1A. The CME system is composed of several main parts: umbrella nozzles, spinning cylinder, temperature controller (TC), electromagnetic heating device (EHD), thermocouple and high voltage generator, etc.

Some components, including the TC and high voltage generator, have been described in our related melt eletrospinning reports [38–40]. The EHD is composed of an electromagnetic heating circle and a fan, located in the lower layer of the spinning cylinder, which affects heating and cooling. The thermocouple feeds back the internal temperature of the cylinder to the TC, and then the TC adjusts the temperature of spinning in real-time. Moreover, two umbrella nozzles fixed on the spinning cylinder and the umbrella spinning nozzle can ensure the high efficiency of this setup. Poly (L-lactic acid) (PLLA, Mn=100000, Tg=61 °C, Tm= 171 °C, Zhejiang Haizheng Biomaterials Co. Ltd., China) was employed as a model polymer to investigate the mechanism of our CME method. The PLLA melt flow rate was maintained as 3–5 g/10 min at 190 °C/2.16 kg.

2.2 Characterization of PLLA fibrous scaffolds

The morphology of our CME-derived PLLA fibrous scaffolds was observed via a scanning electron microscope (SEM, Hitachi S4700, Japan) after gold coating, and the fiber diameters were analyzed by using Image J software. In order to calculate the fiber orientation, SEM images of PLLA fibrous scaffolds were transformed into power spectra using a fast Fourier transform (FFT) method [41, 42]. Based on the power spectra, a radial summation of pixel intensity from 0–360° was conducted using the oval profile plug-in from Image J. The fiber orientation of all samples was determined by the peak characteristics, where the greatest intensity of increase over the smallest degree range signified the highest degree of fiber orientation. The fiber production was measured by a high precision electronic scale (HPES), with the fibers being collected for 30 s for every condition. The pore distribution of the as-prepared PLLA scaffolds was measured by a through-pore size analyzer (POROLUX TM100FM, IB-FT, Germany). The 3D structure of the PLLA fibrous scaffolds were observed by MicroCT test (SkyScan1172, Micro Photonics Inc., USA).

The surface hydrophilicity of all of the samples was measured at room temperature by using a video contact angle instrument (OCA15EC, Germany). Deionized water (3μL) was dropped onto the surface of samples, and a photo was taken after the balancing of the water droplet. For the meshes with aligned fibers, the water contact angles in the direction along with fiber alignment were measured. Three samples in each group were used for the contact angle test. Uniaxial tension tests were performed using a strength tester (XQ-2 strength tester, China). The samples were cut into 30 mm × 3 mm, and the tests were performed with a gauge length of 10 mm at a constant speed of 10 mm/min until failure occurred. For the meshes with aligned fiber morphology, the mechanical properties in the direction along the orientation of the fibers were evaluated. Five samples were used for the mechanical test and measurement.

2.3 Cell seeding, culture and differentiation

Established primary HADMSC (Lonza, USA) were cultured in growth medium (GM) consisting of DMEM/F12 (Invitrogen, USA), 10% FBS (Invitrogen, USA) and 1% P/S (Invitrogen, USA). Tendon differentiation medium (TDM) containing DMEM/F12 medium, 2% FBS, 20 ng/ml TGFβ3 (PeproTech, USA) was used to induce HADMSC differentiation into tenocyte like cells. HUVEC (Lonza, USA) were cultured in endothelial growth medium (EGM) (EGM-2 BulletKit, Lonza, USA). For cell co-culture, HADMSC: HUVEC (4:1)

were cultured in a mixed medium (TDM:EGM=4:1). All of the cells were used at passages 4–6 and cultured in 5% CO_2 at 37 °C. All PLLA fibrous scaffolds were cut into 12 mm × 12 mm rectangular samples. Before cell seeding, the fibrous scaffolds were sterilized in 70% (v/v) ethanol overnight, washed twice in phosphate buffered saline solution (PBS), and then submerged in GM overnight. HADMSC or HADMSC:HUVEC (4:1) was seeded at a density of 1×10^5 cells per fibrous scaffold, and medium was replaced every 2 days.

2.4 Cell viability, morphology and proliferation

The viability and morphology of HADMSC seeded on different scaffolds in TDM through 21 days of culture were characterized by a Live/Dead assay (Invitrogen, USA), as previously described [10]. A confocal laser scanning microscope (CLSM, LSM 710, Carl Zeiss, Germany) was employed to obtain fluorescence images. The cell alignment degree, on both random and aligned scaffolds, was obtained by using Image J. For calculations, 200 different cells were randomly selected and measured. The cell proliferation tests of HADMSC on different scaffolds were conducted on days 7 and 21 by using MTT assay [10].

2.5 Histological and immunofluorescent staining

HADMSC-seeded PLLA aligned scaffolds with three different thicknesses (~200, 400, 800 μm) were cultured in TDM through 21 days, then fixed in 4% paraformaldehyde for 4 hours, and cross-sectioned (~10 μm in thick) using a cryosectioner (Leica, Germany). Cross sections were stained with hematoxylin and eosin (H&E). Image J software was used to threshold the image, measure the area with cells, and assess the cell density in the scaffold cross-sectional direction (cell occupied area/scaffold cross-sectional area). For immunofluorescent staining, cell-seeded scaffolds were fixed in 4% paraformaldehyde, permeabilized in 0.2% Triton X-100, and then blocked with 1% bovine serum albumin (BSA) overnight at 4 °C. The cell-constructs were then treated with primary antibodies to tenomodulin (TNMD, 1:50, Abcam, USA), collagen type I (COL1, 1:100, Santa Cruz Biotechnology, USA), or CD31 (1:100, Cell Signaling, USA) overnight at 4 °C. Secondary fluorescent antibodies were incubated for 2 hours, and nuclear counterstaining (Draq 5, 1:1000, Thermo Scientific, USA) was performed for 30 minutes at room temperature. The stained samples were imaged with the Zeiss 710 CLSM.

2.6 RNA isolation and qPCR

QIA-Shredder and RNeasy mini-kits (QIAgen, USA) were utilized to extract total RNA from cell-seeded constructs, according to the manufacturer's instructions. The total RNA was synthesized into first strand cDNA in a 20 μL reaction, using an iScript cDNA synthesis kit (BioRad Laboratories, USA). Real-time PCR analysis was performed in a StepOnePlus™ Real-Time PCR System (Thermo Scientific, USA), using SsoAdvanced SYBR Green Supermix (Bio-Rad, USA). cDNA samples were analyzed for the gene of interest and for the housekeeping gene 18S rRNA. The level of expression of each target gene was calculated using comparative Ct ($2^{-\Delta\Delta Ct}$) method. All primers used in this study are listed in Supplementary Table S1.

2.7 Statistical Analysis

All quantitative data was expressed as mean ± standard deviation (SD). Pairwise comparisons between groups were conducted using ANOVA with Scheffé post-hoc tests in statistical analysis. A value of $p<0.05$ was considered statistically significant.

3. Results

3.1. Scaffold fabrication, optimization and characterization

An in-house CME system, which combines centrifugal spinning with melt electrospinning, was employed to fabricate environmentally-friendly and solvent-free fibrous meshes (Fig. 1A and Video S1). PLLA fibrous meshes with controlled fiber orientation were manufactured using multiple different spinning parameters (Fig. 1B–D and Fig. S1–3). The fiber orientation was generally improved with the increase of voltage in the range of 5–45 kV (Fig. 1B and Fig. S1). However, the fiber orientation slightly declined when the voltage was too high. The fiber orientation presented a significantly increasing trend with the increase of temperature from 215 to 265 °C (Fig. 1C and Fig. S2). Moreover, the fiber orientation ascended initially, then descended, with increasing rotational speed from 780 to 1500 rpm (Fig. 1D and Fig. S3).

We further evaluated the effects of different parameters on fiber productivity (Fig. 1E–G). Fiber production increased slowly with the increase of voltage, while it increased significantly with the increase of rotational speed (Fig.1E). It was demonstrated that the effect of rotational speed on fiber production was stronger than that of voltage. Fiber production increased significantly with the increase of temperature, indicating that the temperature and rotational speed played the same important roles on fiber production (Fig. 1F). Additionally, when the temperature was above 245 °C, the fiber production kept constant with the increase of rotational speed probably due to the lack of melt material supply. Fig. 1G also demonstrated that the rotational speed was one of main parameters affecting fiber production of the resultant meshes. With the increase of temperature and the initial mass of raw material, fiber production was significantly increased.

The fiber diameters of PLLA meshes were tunable, ranging from several hundred nanometers to ten micrometers by adjusting the CME conditions. To optimize PLLA fibrous scaffolds, the effects of different spinning parameters were also explored and presented in supplementary files (Fig. S4–10). According to the parameter optimization results, a typical, randomly-arranged PLLA fibrous mesh with a mean fiber diameter of 9.71±5.46 μm was fabricated under the process conditions: V=30 kV, R=780 rpm, T=230 °C, C=10 cm, M=6 g and shown in Fig. 2A. As a comparison, a highly-ordered, ultra-fine PLLA fibrous scaffold, with a mean fiber diameter of 5.25±3.04 μm, was prepared under the process conditions: V=35 kV, R=1260 rpm, T=235 °C, C=8 cm, M=6 g and presented in Fig. 2B. The micro CT images and video further demonstrated that these two scaffolds exhibited the significant difference of fiber orientation (Fig. 2C, D and Video S2), and therefore were used to investigate the effects of fiber orientation on cell behaviors. Three aligned PLLA fibrous scaffolds with different thicknesses (~200, 400, and 800 μm) were selected to observe the effect of scaffold thickness on cell behaviors for the remainder of the study. A pore size

distribution test (Fig. 2E) showed that fluffy, PLLA fibrous meshes with a mean pore diameter above 35 μm could be obtained by employing our CME technique.

The physical properties of engineered scaffolds with heterogeneous surface topography are usually orientation-dependent. For the meshes with aligned fibers, both wettability and uniaxial tensile tests were conducted in the direction along the fiber alignment, which is more important for tendon tissue engineering application. The water contact angle measurement was conducted for the PLLA random fibrous scaffold (with a thickness of ~200 μm) and PLLA aligned fibrous scaffolds with different thicknesses (~200, 400, and 800 μm) to investigate the effects of fiber alignment and scaffold thickness on surface hydrophilicity (Fig. 2F). It was demonstrated that the random scaffold was more hydrophobic with a water contact angle higher than that of aligned scaffolds along the fiber alignment direction. Moreover, the contact angles of aligned scaffolds with different thicknesses (~200, 400, and 800 μm) were comparable (137.8 ± 0.9° vs. 138.2 ± 0.6° vs. 138.2± 0.9°), indicating that scaffold thickness had no significant effects on the scaffold hydrophilicity.

In terms of mechanical properties, the results demonstrated that the mechanical properties of scaffolds were significantly dependent on the fiber alignment and overall scaffold thickness. Aligned scaffolds exhibited a significantly higher Young's modulus and ultimate tensile strength in the direction along the fiber alignment, as compared to the random scaffold (Fig. 2G and H). In addition, the Young's modulus and ultimate tensile strength of the aligned scaffolds displayed a notably decreasing trend, with the increasing of the scaffold thickness.

3.2. Fiber alignment promoted HADMSC proliferation, alignment and tenogenic differentiation

HADMSC were seeded on both random and aligned PLLA fibrous scaffolds and cultured in TDM for 21 days to investigate the effect that the fiber orientation has on cell morphology, proliferation, and tenogenic differentiation. Cell viability and morphology were measured based on a live/dead assay in Fig. 3A–D. HADMSC cultured on both random and aligned meshes showed high viability (>95%) in TDM throughout 21 days of culture. HADMSC responded to the fiber-based topographic features in the scaffolds by the contact guidance phenomenon. When cultured on aligned fibers, most cells elongated and aligned along the fiber alignment direction (Fig. 3C, D). More than 90 % of HADMSC were highly aligned along the direction of fiber orientation (within ±20°) on PLLA aligned fibrous scaffolds in Fig. 3E. By contrast, haphazardly distributed cells, with irregular morphologies, were observed on random fibrous scaffolds at different time points (Fig. 3A, B). An MTT assay was utilized to evaluate the proliferation of HADMSC on the random and aligned scaffolds. The results demonstrated that the cell proliferation rate on the aligned scaffold was significantly higher than that on the random fibrous scaffold at days 7 and 21 (Fig. 3F).

The expression of TNMD (a late marker of tenogenic differentiation) on random and aligned fibrous scaffolds was visualized by immunofluorescent staining after 21-day culture (Fig. 4A, B). TNMD was detected on both random and aligned fibrous scaffolds when conditioned in TDM, while the higher TNMD expression was found on the aligned scaffold. Importantly, the fiber alignment in the scaffold can guide the TNMD protein formation

along the arrangement direction of fibers, which can mimic the ECM architecture of native tendon tissues (Fig. S11A). Results from qPCR also confirmed that HADMSC showed higher levels of TNMD gene expression on the aligned fibrous scaffold, compared to HADMSC on the random fibrous scaffold (Fig. 4F). Moreover, the expressions of other tenocyte-related genes, including scleraxis (SCX), COL1, and tenascin-C (TNC), in the aligned scaffold group were also significantly higher than that of the random scaffold group (Fig. 4C, D and G). These results demonstrated that the HADMSC exhibited more tenogenic phenotypes when conditioned on the aligned scaffold. These results supported that the aligned PLLA fibrous scaffold provided a more appropriate microenvironment to promote high cell viability, proliferation, and tenogenic differentiation of HADMSC.

3.3 Thinner scaffolds promoted HADMSC infiltration

To evaluate how scaffold thickness affects cell migration and proliferation, HADMSC were seeded and cultured on PLLA aligned scaffolds with three different thicknesses (~200, 400, and 800 μm) in TDM for 21 days. Cross-sectional H&E staining images of three cell-seeded scaffolds were shown in Fig. 5A–C. The cells attached and grew on the scaffold surface, as well as penetrated inside the scaffold through the homogenously distributed pores between fibers. After 21 days of culture, the highest cell density was detected on the thinnest scaffold, and the cell density decreased with increasing scaffold thickness (Fig. 5D). An MTT assay showed that the cells cultured on the thinnest scaffolds possessed a significantly accelerated proliferation rate at early 7-day culture (Fig. 5E). However, the cell number was similar on scaffolds with different thicknesses after 21-day culture. These results indicated that the thin scaffold provided better support for early cell proliferation than the thick scaffold. In addition, although the cell density decreased with increasing scaffold thickness, the overall cell numbers were probably comparable in the scaffolds with various thicknesses, due to the volume and area increase.

3.4 HADMSC-HUVEC co-culture promoted in vitro tenogenic differentiation of HADMSC

Next, we evaluated the protein and gene expression of HADMSC and HADMSC-HUVEC co-culture (4:1 ratio) on aligned fibrous scaffolds in different conditioning media and determined whether co-culture affected tenogenic differentiation in vitro. In TDM, HADMSC alone were negative to CD31 (vascularization related protein) (Fig. 6A). The addition of endothelial growth medium (EGM, TDM:EGM=4:1) significantly promoted the TNMD and COL1 protein expression of HADMSC (Fig. 6C & D), but HADMSC were still expressed very limited CD31 in the hybrid media. For the co-culture system, TNMD and COL1 were expressed robustly, and obvious CD31 expression was observed (Fig. 6E & F). In native adult tendon, TNMD expression was also robust, and significant CD31 expression was also detected, as shown in Fig. S11. Results from qPCR showed that both the EGM addition and HADMSC-HUVEC co-culture significantly upregulated the TNC gene (Fig. 6G), but no statistical difference was observed between these two conditions.

4. Discussion

In this study, a novel CME setup was developed and implemented to fabricate organic solvent free, diameter and thickness controllable fibrous scaffolds. Our CME combined the

advantages of centrifugal spinning, electrospinning, and accurate temperature control technology, which showed three notable advantages. First, this technology can directly employ thermoplastic biopolymers to prepare fibers, without utilizing solvent to dissolve polymers. This process not only saves on the cost and time, but also eliminates the side effects of any solvent. The CME system provides an effective method to solve the solvent residue issue of traditional electrospun fibers. Second, some raw materials cannot be spun by traditional electrospinning, due to the lack of an appropriate solvent. Our CME technology can utilize the melting of polymeric materials for spinning, which broadened the scope of choice of raw materials which can be used. Furthermore, by using this CME system, we can fabricate fiber meshes with controllable thickness, which facilitates cell migration and infiltration into the inner layers of scaffolds. Finally, Our CME showed obviously high spinning efficiency (~ 3 g/min), which increased to more than 1000-fold compared with the typical needle-based electrospinning setup. In this study, we fabricated PLLA fibrous meshes with controlled fiber diameter, orientation, and thickness by the adjustment of the appropriate spinning parameters. PLLA was chosen as the biomaterial for the tendon regeneration application because it is a fully biocompatible, biodegradable, synthetic material which can undergo remodeling and ultimately be replaced by regenerated tissue in vivo [43, 44]. In addition, PLLA is thermoplastics and it can be heated to its melting point, cooled, and reheated again without significant degradation [45].

To generate engineered tendon tissue, biomimicking of the specific topography of native tendon ECM structure is of significant importance. Our present results demonstrated that aligned fibers can guide HADSMC alignment and synthesis of a tendon-like ECM containing oriented TNMD and collagen. Moreover, our current study showed that the aligned fibers promoted the proliferation and tenogenic differentiation of HADMSC, when compared with the cells on random fibers. Some other studies also confirmed that aligned topography guides cell alignment and organization and guides collagen fibril formation along the arrangement direction of fibers [18, 46].

Cell migration and infiltration are critically important for the practical application of engineered tissue grafts. Typical electrospinning processes usually produce tightly packed, mesh-like fibrous meshes with compact, 2D construction and poor controllability. The fibrous meshes fabricated by typical electrospinning usually possess a pore diameter below 5 μm [47–50]. These structure features further limit cell growth to only on the superficial surface, rather than infiltrating into the inner layers [51–53]. To overcome this great obstacle, some extra post-treatments with complicated procedures, such as salt leaching/ gas foaming technique [54], ultrasonication [55], and freeze drying process [56], have been developed to enhance cellular ingrowth into the scaffolds. Our CME system enables the fabrication of fibrous scaffolds with controllable thickness and a fluffy texture. The pore size distribution test showed that our CME-fabricated, PLLA fibrous scaffolds possessed a mean pore diameter above 35 μm, which was large enough for cell infiltration. Cross-sectional H&E staining and immunofluorescent staining of HADSMC-seeded scaffolds, with three different thicknesses, suggested that the cells successfully proliferated and infiltrated throughout the bulk PLLA fibrous scaffolds. Although the scaffold thickness affected the cell proliferation rate at the early stage of cell culture, the cell numbers tended to be similar after longer culture time. These results indicate that it is feasible to construct a 3D tissue

graft for tendon repair by using our CME-made PLLA aligned scaffolds with various thicknesses. For the future in vivo implantation, the scaffolds with high thickness would provide more spaces for cell penetration and proliferation.

Limited vascularization and low vascular supply may be crucial factors that delay the healing of tendon-related diseases or injuries. During the early stage of healing after tendon injury and rupture, there is an initial, robust vascular response with increased VEGF expression, then predictably drops off with time [57]. Several studies also reported that hypervascularization was observed after initial implantation, which diminished to native tendon levels at a late stage of healing [31, 37]. These results indicate that neovascularization is a natural healing process and may be essential for long term survival of grafts. Endothelial cells (EC) play an important role in constructing the vascular structure and maintaining vascular function [57–59]. Recent investigations have indicated that the appropriate co-cultured cells could release humoral factors, which further influence the expansion and differentiation of mesenchymal stem cells (MSC) [60–62]. Some co-culture studies have also shown that close cell-to-cell contact in culture enhanced specific cell lineage formation [63–65]. In the present study, HUVEC were utilized to co-culture with HADMSC on PLLA fibrous scaffolds with aligned fiber architectures. We investigated the feasibility of using the HADMSC and HUVEC co-culture system to induce the differentiation of HADMSC for constructing the tissue-engineered tendon in vitro. The HADMSC and HUVEC co-culture system was demonstrated to promote in vitro HADMSC differentiation towards tenocytes on the aligned PLLA fibrous scaffold. Some other studies also employed a co-culture technique to promote MSC differentiation, and confirmed that a co-culture of MSC and tenocytes enhanced the tenogenic differentiation of MSC [66–69]. Our results indicate that the incorporation of EC may initiate the vascularization and promote tenogenesis of MSC to recapitulate the initial tendon healing process. The ratio of EC and the crosstalk between EC and HADMSC and/or tenocytes should be further investigated and optimized to maximize function of vascularization. In addition, temporal and spatial control of vascularization is also important to prevent hypervascularity and inhibit scar formation.

Conclusions

In our current study, a novel CME system was developed to fabricate solvent-free, micro-/nano-fibrous meshes with controlled fiber alignment and mesh thickness. PLLA was employed as a model polymer to explore and investigate the effect of the spinning conditions on fiber properties. Compared with random PLLA fibrous scaffolds, the obtained, highly-ordered meshes could better mimic the native tendon ECM structure by facilitating the HADMSC orientation, proliferation, and differentiation towards tendon fibroblasts. Moreover, the relatively fluffy fibrous scaffolds, with controllable thickness, were fabricated by our CME technique. These meshes were beneficial for the cell migration and infiltration into the inner layers of scaffolds and further formation of 3D tendon grafts. The co-culture of HADMSC and HUVEC promoted in vitro tenogenic differentiation of HADMSC. Therefore, our living, aligned fibrous scaffolds, fabricated by our CME system, are promising as tendon grafts that mimic the native tendon tissue-like architecture, anisotropy, and cell phenotype, as well as promote the natural healing process.

Supplementary Material

Refer to Web version on PubMed Central for supplementary material.

Acknowledgments

This work has been supported by Mary & Dick Holland Regenerative Medicine Program start-up grant and Nebraska Research Initiative funding. This study was also financially supported by the National Natural Science Foundation of China (21374008). We would like to thank Janice A. Taylor and James R. Talaska of the Advanced Microscopy Core Facility at the University of Nebraska Medical Center (UNMC) for providing assistance with confocal microscopy. Support for the UNMC Advanced Microscopy Core Facility was provided by the Nebraska Research Initiative, the Fred and Pamela Bvvuffett Cancer Center Support Grant (P30CA036727), and an Institutional Development Award (IDeA) from the NIGMS of the NIH (P30GM106397). We also would like to thank Xin Wei and Xiaoyan Wang at Department of Pharmaceutical Sciences of the University of Nebraska Medical Center (UNMC) for providing assistance with Micro CT imaging.

References

1. Lomas A, Ryan C, Sorushanova A, Shologu N, Sideri A, Tsioli V, Fthenakis GC, Tzora A, Skoufos I, Quinlan LR, O'laighin G. The past, present and future in scaffold-based tendon treatments. Advanced drug delivery reviews. 2015; 84:257–277. [PubMed: 25499820]
2. Wong R, Alam N, McGrouther A, Wong J. Tendon grafts: their natural history, biology and future development. Journal of Hand Surgery (European Volume). 2015; 40:669–681.
3. Thomopoulos S, Parks WC, Rifkin DB, Derwin KA. Mechanisms of tendon injury and repair. Journal of Orthopaedic Research. 2015; 33:832–839. [PubMed: 25641114]
4. Tellado SF, Balmayor ER, Van Griensven M. Strategies to engineer tendon/ligament-to-bone interface: Biomaterials, cells and growth factors. Advanced drug delivery reviews. 2015; 94:126–140. [PubMed: 25777059]
5. Yin Z, Chen X, Chen Jl, Ouyang HW. Stem cells for tendon tissue engineering and regeneration. Expert opinion on biological therapy. 2010; 10:689–700. [PubMed: 20367125]
6. Hakimi O, Mouthuy P, Zargar N, Lostis E, Morrey M, Carr A. A layered electrospun and woven surgical scaffold to enhance endogenous tendon repair. Acta biomaterialia. 2015; 26:124–135. [PubMed: 26275911]
7. Zhang W, Yang Y, Zhang K, Li Y, Fang G. Weft-knitted silk-poly (lactide-co-glycolide) mesh scaffold combined with collagen matrix and seeded with mesenchymal stem cells for rabbit Achilles tendon repair. Connective tissue research. 2015; 56:25–34. [PubMed: 25333819]
8. Huang X, Huang G, Ji Y, guang Ao R, Yu B, long Zhu Y. Augmented Repair of Acute Achilles Tendon Rupture Using an Allograft Tendon Weaving Technique. The Journal of Foot and Ankle Surgery. 2015; 54:1004–1009. [PubMed: 26015299]
9. Aibibu D, Hild M, Cherif C. An overview of braiding structure in medical textile: fiber-based implants and tissue engineering. Advances in Braiding Technology: Specialized Techniques and Applications. 2016; 171
10. Wu SH, Duan B, Liu PH, Zhang CD, Qin XH, Butcher JT. Fabrication of Aligned Nanofiber Polymer Yarn Networks for Anisotropic Soft Tissue Scaffolds. ACS Applied Materials & Interfaces. 2016; 8:16950–16960. [PubMed: 27304080]
11. Wu SH, Qin XH. Uniaxially aligned polyacrylonitrile nanofiber yarns prepared by a novel modified electrospinning method. Materials Letters. 2013; 106:204–207.
12. Wu SH, Qin XH, Li M. The structure and properties of cellulose acetate materials: A comparative study on electrospun membranes and casted films. Journal of Industrial Textiles. 2014; 44:85–98.
13. Cui W, Zhou Y, Chang J. Electrospun nanofibrous materials for tissue engineering and drug delivery. Science and Technology of Advanced Materials. 2016; 11:014108.
14. Khorshidi S, Solouk A, Mirzadeh H, Mazinani S, Lagaron JM, Sharifi S, Ramakrishna S. A review of key challenges of electrospun scaffolds for tissue-engineering applications. Journal of tissue engineering and regenerative medicine. 2015; 10:715–738. [PubMed: 25619820]

15. Zhang X, Bogdanowicz D, Erisken C, Lee NM, Lu HH. Biomimetic scaffold design for functional and integrative tendon repair. Journal of Shoulder and Elbow Surgery. 2012; 21:266–277. [PubMed: 22244070]
16. Domingues R, Chiera S, Gershovich P, Motta A, Reis RL, Gomes ME. Enhancing the Biomechanical Performance of Anisotropic Nanofibrous Scaffolds in Tendon Tissue Engineering: Reinforcement with Cellulose Nanocrystals. Advanced healthcare materials. 2016; 5:1364–1375. [PubMed: 27059281]
17. Zhang C, Yuan H, Liu H, Chen X, Lu P, Zhu T, Yang L, Yin Z, Heng BC, Zhang Y, Ouyang H. Well-aligned chitosan-based ultrafine fibers committed teno-lineage differentiation of human induced pluripotent stem cells for Achilles tendon regeneration. Biomaterials. 2015; 53:716–730. [PubMed: 25890767]
18. Wang W, He J, Feng B, Zhang Z, Zhang W, Zhou G, Cao Y, Fu W, Liu W. Aligned nanofibers direct human dermal fibroblasts to tenogenic phenotype in vitro and enhance tendon regeneration in vivo. Nanomedicine. 2016; 11:1055–1072. [PubMed: 27074092]
19. Sensini A, Gualandi C, Cristofolini L, Tozzi G, Dicarlo M, Teti G, Mattioli-Belmonte M, Focarete ML. Biofabrication of bundles of poly (lactic acid)-collagen blends mimicking the fascicles of the human Achille tendon. Biofabrication. 2017; 9:015025. [PubMed: 28224971]
20. Mouthuy PA, Zargar N, Hakimi O, Lostis E, Carr A. Fabrication of continuous electrospun filaments with potential for use as medical fibres. Biofabrication. 2015; 7:025006. [PubMed: 25987265]
21. Chao PH, Hsu HY, Tseng HY. Electrospun microcrimped fibers with nonlinear mechanical properties enhance ligament fibroblast phenotype. Biofabrication. 2014; 6:035008. [PubMed: 24867684]
22. Lui YS, Lewis MP, Loo SC. Sustained-release of naproxen sodium from electrospun - aligned PLLA-PCL scaffolds. Journal of tissue engineering and regenerative medicine. 2017; 11:1011–1021. [PubMed: 25712012]
23. Song J, Gao H, Zhu G, Cao X, Shi X, Wang Y. The construction of three-dimensional composite fibrous macrostructures with nanotextures for biomedical applications. Biofabrication. 2016; 8:035009. [PubMed: 27563025]
24. Lee H, Ahn S, Choi H, Cho D, Kim G. Fabrication, characterization, and in vitro biological activities of melt-electrospun PLA micro/nanofibers for bone tissue regeneration. Journal of Materials Chemistry B. 2013; 1:3670–3677.
25. Liu Y, Cui H, Zhuang X, Wei Y, Chen X. Electrospinning of aniline pentamer-graft-gelatin/PLLA nanofibers for bone tissue engineering. Acta biomaterialia. 2014; 10:5074–5080. [PubMed: 25200841]
26. Nam J, Huang Y, Agarwal S, Lannutti J. Materials selection and residual solvent retention in biodegradable electrospun fibers. Journal of applied polymer science. 2008; 7:1547–1554.
27. Soliman S, Pagliari S, Rinaldi A, Forte G, Fiaccavento R, Pagliari F, Franzese O, Minieri M, Di Nardo P, Licoccia S, Traversa E. Multiscale three-dimensional scaffolds for soft tissue engineering via multimodal electrospinning. Acta biomaterialia. 2010; 6:1227–1237. [PubMed: 19887125]
28. Shao J, Chen S, Du C. Citric acid modification of PLLA nano-fibrous scaffolds to enhance cellular adhesion, proliferation and osteogenic differentiation. Journal of Materials Chemistry B. 2015; 3:5291–5299.
29. Sebe I, Szabó B, Nagy ZK, Szabó D, Zsidai L, Kocsis B, Zelkó R. Polymer structure and antimicrobial activity of polyvinylpyrrolidone-based iodine nanofibers prepared with highspeed rotary spinning technique. International journal of pharmaceutics. 2013; 458:99–103. [PubMed: 24140543]
30. Li Q, Dong L, Li L, Su X, Xie H, Xiong C. The effect of the addition of carbon nanotube fluids to a polymeric matrix to produce simultaneous reinforcement and plasticization. Carbon. 2012; 50:2056–2060.
31. Tempfer H, Traweger A. Tendon Vasculature in Health and Disease. Frontiers in physiology. 2015; 6:330. [PubMed: 26635616]
32. Oryan A, Shoushtari A. Histology and ultrastructure of the developing superficial digital flexor tendon in rabbits. Anatomia, histologia, embryologia. 2008; 37:134–140.

33. Pufe T, Petersen W, Tillmann B, Mentlein R. The angiogenic peptide vascular endothelial growth factor is expressed in foetal and ruptured tendons. Virchows Archiv. 2001; 439:579–585. [PubMed: 11710646]
34. Pufe T, Petersen W, Mentlein R, Tillmann B. The role of vasculature and angiogenesis for the pathogenesis of degenerative tendons disease. Scandinavian journal of medicine & science in sports. 2005; 15:211–222. [PubMed: 15998338]
35. Andarawis-Puri N, Flatow EL, Soslowsky LJ. Tendon basic science: Development, repair, regeneration, and healing. Journal of Orthopaedic Research. 2015; 33:780–784. [PubMed: 25764524]
36. Tempfer H, Wagner A, Gehwolf R, Lehner C, Tauber M, Resch H, Bauer HC. Perivascular cells of the supraspinatus tendon express both tendon-and stem cell-related markers. Histochemistry and cell biology. 2009; 131:733–741. [PubMed: 19280209]
37. Zumstein MA, Rumian A, Lesbats V, Schaer M, Boileau P. Increased vascularization during early healing after biologic augmentation in repair of chronic rotator cuff tears using autologous leukocyte-and platelet-rich fibrin (L-PRF): a prospective randomized controlled pilot trial. Journal of Shoulder and Elbow Surgery. 2014; 23:3–12. [PubMed: 24331121]
38. Xie G, Chen Z, Ramakrishna S, Liu Y. Orthogonal design preparation of phenolic fiber by melt electrospinning. Journal of Applied Polymer Science. 2015; 132:42574.
39. Xie G, Wang Y, Han X, Gong Y, Wang J, Zhang J, Deng D, Liu Y. Pulsed Electric Fields on Poly-L-(lactic acid) Melt Electrospun Fibers. Industrial & Engineering Chemistry Research. 2016; 55:7116–7123.
40. Li X, Liu Y, Peng H, Ma X, Fong H. Effects of hot airflow on macromolecular orientation and crystallinity of melt electrospun poly (L-lactic acid) fibers. Materials Letters. 2016; 176:194–198.
41. Erickson AE, Edmondson D, Chang F-C, Wood D, Gong A, Levengood SL, Zhang M. High-throughput and high-yield fabrication of uniaxially-aligned chitosan-based nanofibers by centrifugal electrospinning. Carbohydrate polymers. 2015; 134:467–474. [PubMed: 26428148]
42. Ayres C, Bowlin GL, Henderson SC, Taylor L, Shultz J, Alexander J, Telemeco TA, Simpson DG. Modulation of anisotropy in electrospun tissue-engineering scaffolds: analysis of fiber alignment by the fast Fourier transform. Biomaterials. 2006; 27:5524–5534. [PubMed: 16859744]
43. Rothrauff BB, Lauro BB, Yang G, Debski RE, Musahl V, Tuan R. Braided and Stacked Electrospun Nanofibrous Scaffolds for Tendon and Ligament Tissue Engineering. Tissue Engineering, 2017. 2017; doi: 10.1089/ten.tea.2016.0319
44. Baek J, Chen X, Sovani S, Jin S, Grogan SP, D'Lima DD. Meniscus tissue engineering using a novel combination of electrospun scaffolds and human meniscus cells embedded within an extracellular matrix hydrogel. Journal of Orthopaedic Research. 2015; 33:572–583. [PubMed: 25640671]
45. Bajpai PK, Singh I, Madaan J. Development and characterization of PLA-based green composites: A review. Journal of Thermoplastic Composite Materials. 2014; 27:52–81.
46. Argento G, de Jonge N, Söntjens S, Oomens C, Bouten C, Baaijens F. Modeling the impact of scaffold architecture and mechanical loading on collagen turnover in engineered cardiovascular tissues. Biomechanics and modeling in mechanobiology. 2015; 14:603–613. [PubMed: 25319256]
47. Bagherzadeh R, Najar SS, Latifi M, Kong L. A theoretical analysis and prediction of pore size and pore size distribution in electrospun multilayer nanofibrous materials. Journal of Biomedical Materials Research Part A. 2013; 101:2107–2117. [PubMed: 23426993]
48. Liu Y, Wang R, Ma H, Hsiao BS, Chu B. High-flux microfiltration filters based on electrospun polyvinylalcohol nanofibrous membranes. Polymer. 2013; 54:548–556.
49. Ma H, Hsiao BS, Chu B. 452 Functionalized electrospun nanofibrous microfiltration membranes for removal of bacteria and viruses. Journal of Membrane Science. 2014:446–452.
50. Jia L, Prabhakaran MP, Qin X, Ramakrishna S. Stem cell differentiation on electrospun nanofibrous substrates for vascular tissue engineering. Materials Science and Engineering: C. 2013; 33:4640–4650. [PubMed: 24094171]
51. Yang C, Deng G, Chen W, Ye X, Mo X. A novel electrospun-aligned nanoyarn-reinforced nanofibrous scaffold for tendon tissue engineering. Colloids and Surfaces B: Biointerfaces. 2014; 122:270–276. [PubMed: 25064476]

52. Blakeney BA, Tambralli A, Anderson JM, Andukuri A, Lim D-J, Dean DR, Jun HW. Cell infiltration and growth in a low density, uncompressed three-dimensional electrospun nanofibrous scaffold. Biomaterials. 2011; 32:1583–1590. [PubMed: 21112625]
53. Lee JB, Jeong SI, Bae MS, Yang DH, Heo DN, Kim CH, Alsberg E, Kwon IK. Highly porous electrospun nanofibers enhanced by ultrasonication for improved cellular infiltration. Tissue Engineering Part A. 2011; 17:2695–2702. [PubMed: 21682540]
54. Jin G, Shin M, Kim SH, Lee H, Jang JH. SpONGE: spontaneous organization of numerous-layer generation by electrospray. Angewandte Chemie International Edition. 2015; 54:7587–7591. [PubMed: 25958994]
55. Jeong SI, Burns NA, Bonino CA, Kwon IK, Khan SA, Alsberg E. Improved cell infiltration of highly porous 3D nanofibrous scaffolds formed by combined fiber-fiber charge repulsions and ultra-sonication. Journal of Materials Chemistry B. 2014; 2:8116–8122. [PubMed: 25530854]
56. Cui Z, Zhao H, Peng Y, Han J, Turng LS, Shen C. Fabrication and Characterization of Highly Porous Chitosan/Poly (DL lactic-co-glycolic acid) Nanocomposite Scaffolds Using Electrospinning and Freeze Drying. Journal of Biobased Materials and Bioenergy. 2014; 8:281–291.
57. Fealy S, Adler RS, Drakos MC, Kelly AM, Allen AA, Cordasco FA, Warren RF, O'Brien SJ. Patterns of vascular and anatomical response after rotator cuff repair. American Journal of Sports Medicine. 2006; 34:120–127. [PubMed: 16260468]
58. Watson EC, Koenig MN, Grant ZL, Whitehead L, Trounson E, Dewson G, Coultas L. Apoptosis regulates endothelial cell number and capillary vessel diameter but not vessel regression during retinal angiogenesis. Development. 2016; 143:2973–2982. [PubMed: 27471260]
59. Jaffe, EA. Biology of endothelial cells. Vol. 27. Springer Science & Business Media; 2012.
60. Kim J, Kim HN, Lim K-T, Kim Y, Pandey S, Garg P, Choung YH, Choung PH, Suh KY, Chung JH. Synergistic effects of nanotopography and co-culture with endothelial cells on osteogenesis of mesenchymal stem cells. Biomaterials. 2013; 34:7257–7268. [PubMed: 23834896]
61. Paschos NK, Brown WE, Eswaramoorthy R, Hu JC, Athanasiou KA. Advances in tissue engineering through stem cell - based co - culture. Journal of tissue engineering and regenerative medicine. 2015; 9:488–503. [PubMed: 24493315]
62. Cun X, Xie J, Lin S, Fu N, Deng S, Xie Q, Zhong J, Lin Y. Gene profile of soluble growth factors involved in angiogenesis, in an adipose-derived stromal cell/endothelial cell co-culture, 3D gel model. Cell proliferation. 2015; 48:405–412. [PubMed: 26037311]
63. Wang INE, Bogdanowicz DR, Mitroo S, Shan J, Kala S, Lu HH. Cellular interactions regulate stem cell differentiation in tri-culture. Connective Tissue Research. 2016; 57:476–487. [PubMed: 27599920]
64. Bogdanowicz DR, Lu HH. Multifunction co-culture model for evaluating cell–cell interactions. Biomimetics and Stem Cells: Methods and Protocols. 2014:29–36.
65. Bogdanowicz DR, Lu HH. Studying cell - cell communication in co - culture. Biotechnology Journal. 2013; 8:395–396. [PubMed: 23554248]
66. Luo Q, Song G, Song Y, Xu B, Qin J, Shi Y. Indirect co-culture with tenocytes promotes proliferation and mRNA expression of tendon/ligament related genes in rat bone marrow mesenchymal stem cells. Cytotechnology. 2009; 61:1–10. [PubMed: 19842053]
67. Schneider PR, Buhrmann C, Mobasheri A, Matis U, Shakibaei M. Three dimensional high density co-culture with primary tenocytes induces tenogenic differentiation in mesenchymal stem cells. Journal of Orthopaedic Research. 2011; 29:1351–1360. [PubMed: 21437969]
68. Fan H, Liu H, Toh SL, Goh JC. Enhanced differentiation of mesenchymal stem cells co-cultured with ligament fibroblasts on gelatin/silk fibroin hybrid scaffold. Biomaterials. 2008; 29:1017–1027. [PubMed: 18023476]
69. Barboni B, Curini V, Russo V, Mauro A, Di Giacinto O, Marchisio M, Alfonsi M, Mattioli M. Indirect co-culture with tendons or tenocytes can program amniotic epithelial cells towards stepwise tenogenic differentiation. PLoS One. 2012; 7:e30974. [PubMed: 22348033]

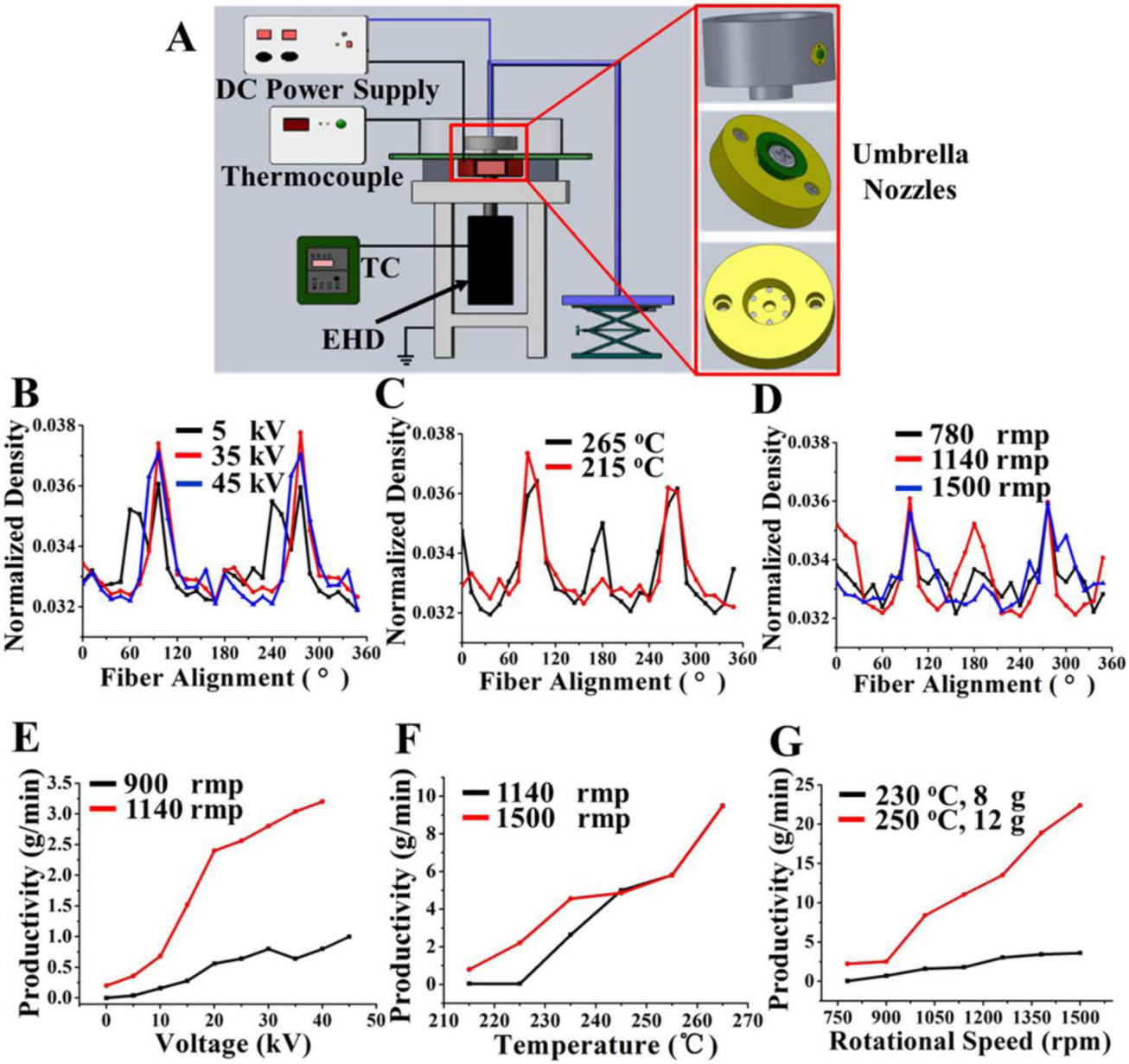

Figure 1.

Fabrication of PLLA fibrous scaffolds by using CME system. (A) Schematic of our CME experimental setup. (B) Variation of the fiber alignment as a function of spinning voltages at 5 kV, 35 kV, and 45 kV. Other spinning parameters were maintained constant: T=230 °C, C=10 cm, R=900 rpm. (C) Variation of the fiber alignment as a function of spinning temperatures at 265 °C and 215 °C. Other spinning parameters were maintained constant: V=35 kV, C=10 cm, R=1140 rpm. (D) Variation of the fiber alignment as a function of spinning rotational speeds at 780 rpm, 1140 rpm, and 1500 rpm. Other spinning parameters were maintained constant: V=30 kV, C=10 cm, T=230 °C. (E) Fiber productivity as a function of voltage (0–50 kV). Curves shown for rotational speeds of 900 rpm and 1140 rpm. Other parameters were maintained constant: T=230 °C, C=10 cm, M=8 g; (F) Fiber

productivity as a function of temperature (215–265°C). Curves shown for rotational speeds of 1140 rpm and 1500 rpm. Other parameters were maintained constant: 35 kV, C=10 cm, M=8 g; (G) Fiber productivity as a function of rotational speed (780 rpm-1500 rpm). Curves shown for (1) T=230 °C, M=8 g. (2) T=250 °C, M=12 g. Other parameters were maintained constant: C=10 cm, V=30 kV, R=780 rpm-1500 rpm. “T, R, V, C, M, P” represented the spinning temperature, rotational speed, voltage, the distance of collection, the initial mass of raw PLLA materials, and the production rate of fibers, respectively.

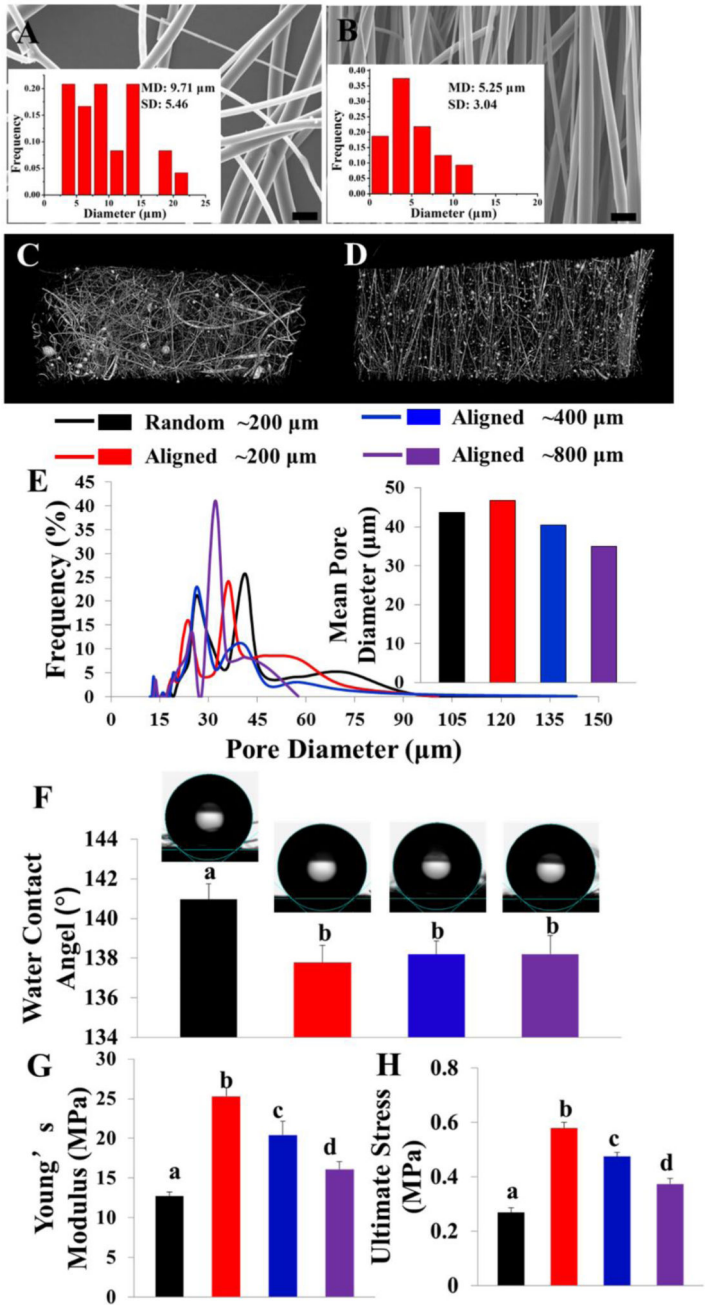

Figure 2.

SEM image and Fiber diameter distribution evaluation of (A) typically random PLLA fibrous scaffold and (B) optimized aligned PLLA fibrous scaffold. Scale bars = 20 μm. Micro CT images of random (C) and aligned (D) PLLA fibrous scaffolds. (E) Pore size distribution and mean pore diameter tests of PLLA fibrous scaffolds with different fiber arrangements (random or aligned) and scaffold thickness (~200 μm, ~400 μm, ~800 μm). (F) Water contact angle of PLLA fibrous scaffolds with different fiber arrangements (random or aligned) and scaffold thickness (~200 μm, ~400 μm, ~800 μm) (n=3; bars that do not share letters are significantly different from each other, $p < 0.01$). The Tensile mechanical tests: (G)

Young's modulus; (H) Tensile strength. (n=5; bars that do not share letters are significantly different from each other, $p < 0.05$)

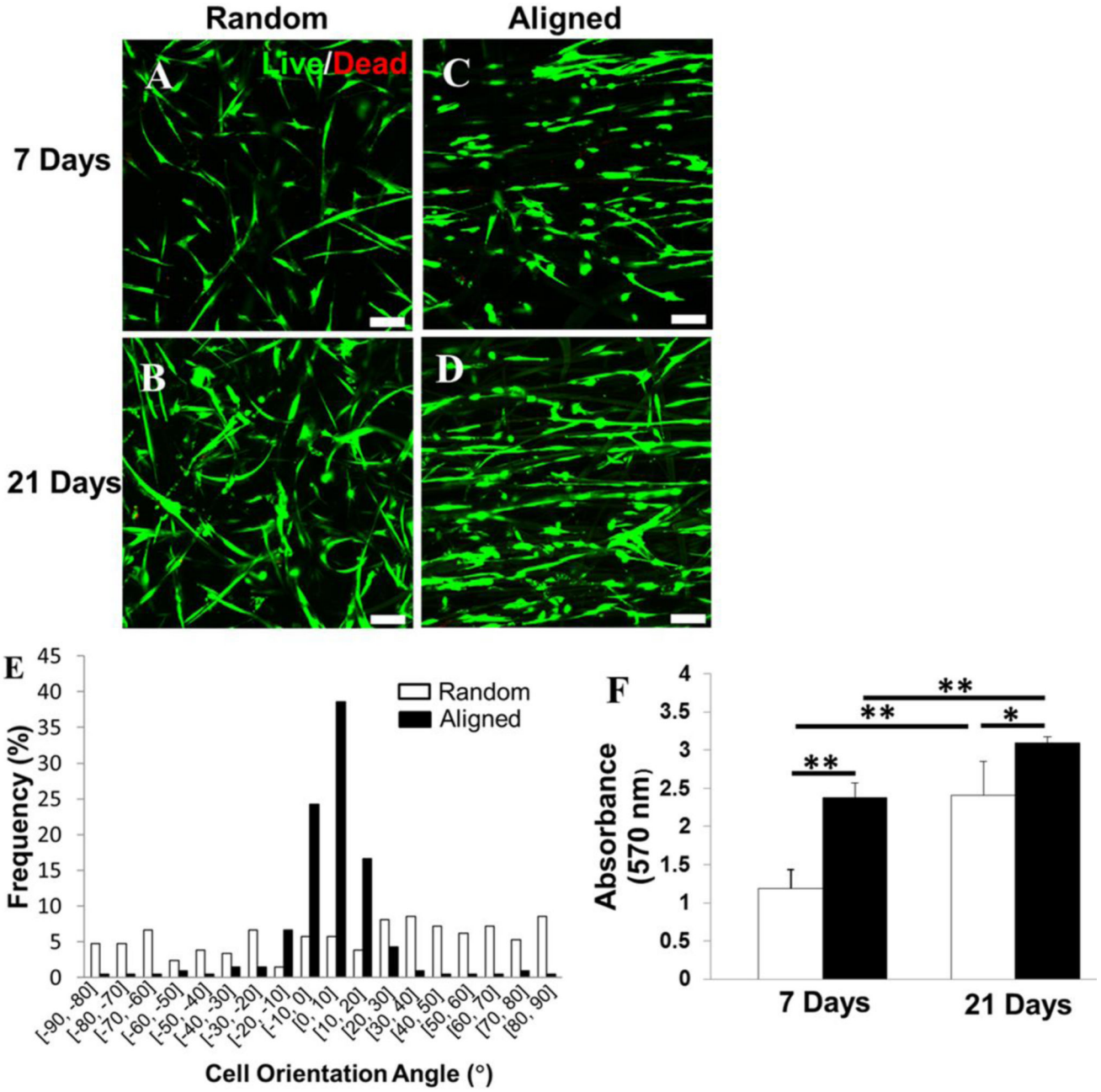

Figure 3.

Fiber alignment induced cell alignment and promoted cell proliferation. Live/Dead images for HADMSC-seeded (A, B) random PLLA fibrous scaffold and (C, D) aligned one conditioned in TDM for 7 days and 21 days. Scale bars = 100 μm. (E) HADMSC cell orientation angle distribution measurement on random and aligned PLLA fibrous scaffolds after 21-day culture in TDM. (F) Cell proliferation quantification by MTT assay at day 7 and 21 on the random and aligned PLLA scaffolds populated with HADMSC in TDM (n=6; *p<0.05, **p<0.01).

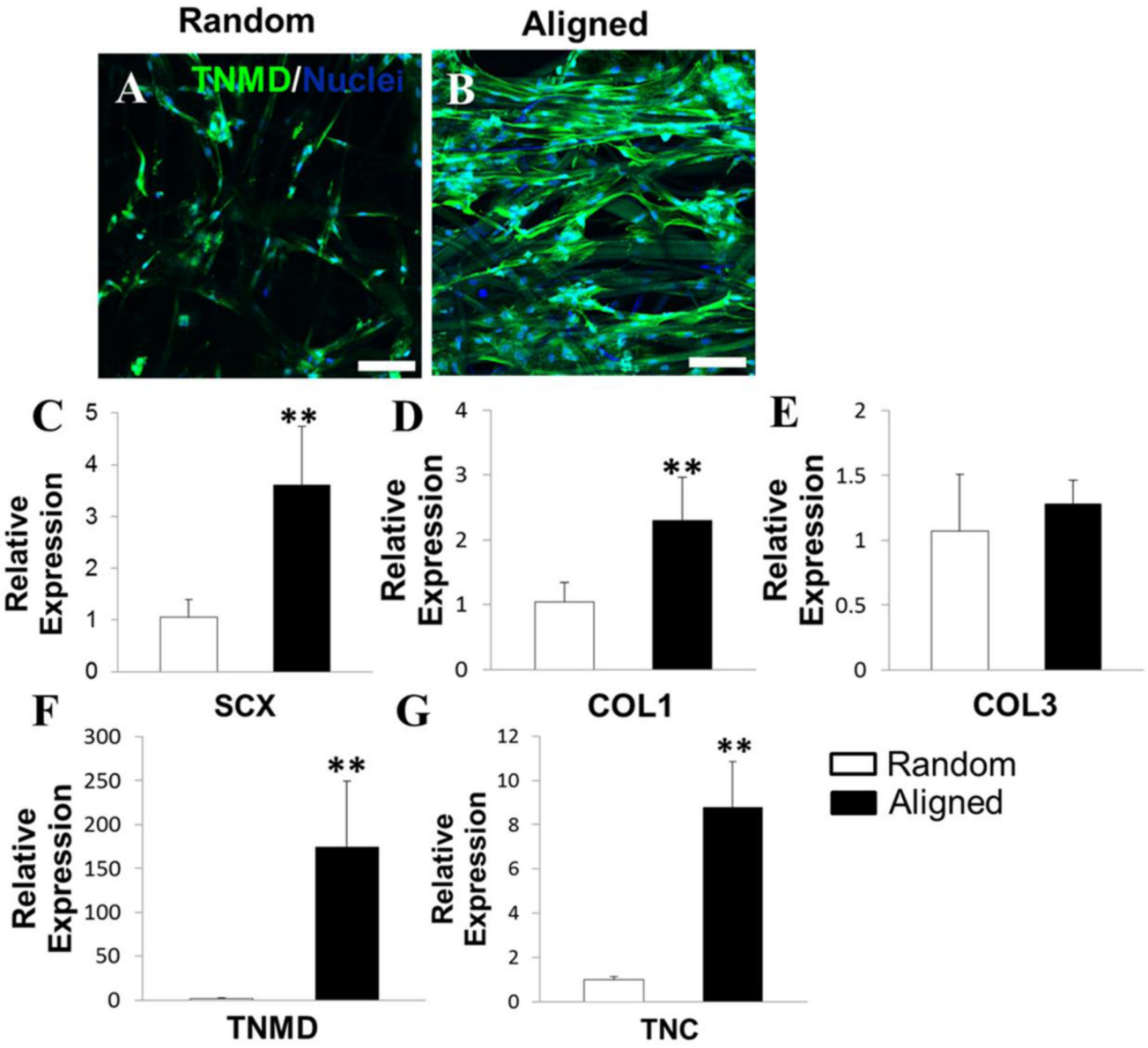

Figure 4.

Fiber alignment promoted HADMSC differentiation towards tenocytes in TDM after 21-day culture. Immunofluorescent staining for TNMD (green) and nuclei (blue) on (A) random PLLA fibrous scaffold and (B) aligned PLLA fibrous scaffold in TDM. Scale bars = 100 μm. Real-time PCR analysis of (C) SCX, (D) COL1, (E) COL3, (F) TNMD and (G) TNC on HADMSC-seeded PLLA random and aligned fibrous scaffolds conditioned in TDM for 21 days. Relative gene expression is presented as normalized to 18S and expressed relative to HADMSC-seeded PLLA random fibrous scaffolds (n=3; ** p<0.01).

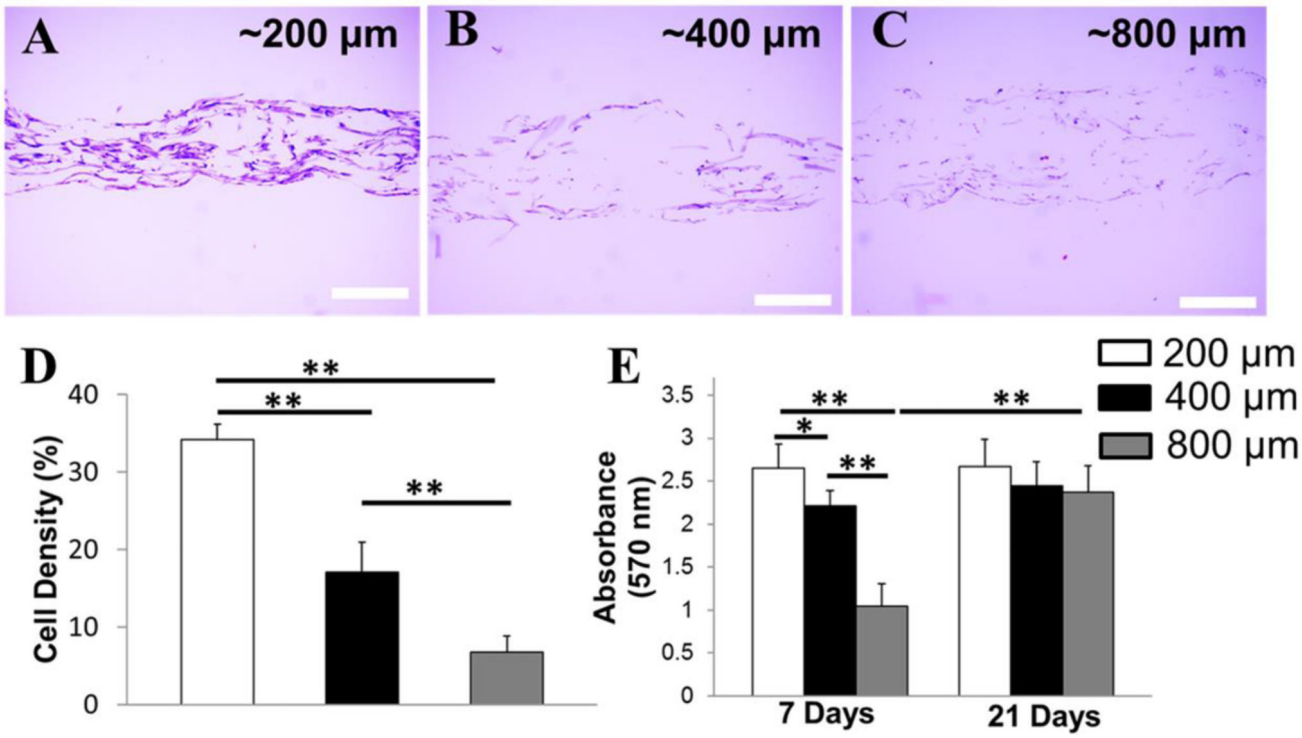

Figure 5.

Thinner scaffolds promoted HADMSC infiltration and proliferation at early stage of cell culture. Cross-sectional H&E staining of HADMSC seeded PLLA aligned fibrous scaffolds with different thickness in TDM for 21 days: (A) ~200 μm, (B) ~400 μm (C) ~800 μm. Scale bars = 200 μm. (D) Cell density at 21 days of aligned in TDM HADMSC-seeded PLLA fibrous scaffolds with different thicknesses (n=5; ** $p<0.01$). (E) Quantification of cell proliferation by MTT assay at day 7 and 21 for aligned in TDM HADMSC-seeded PLLA aligned fibrous scaffolds with different thicknesses (n=6; *$p<0.05$, **$p<0.01$).

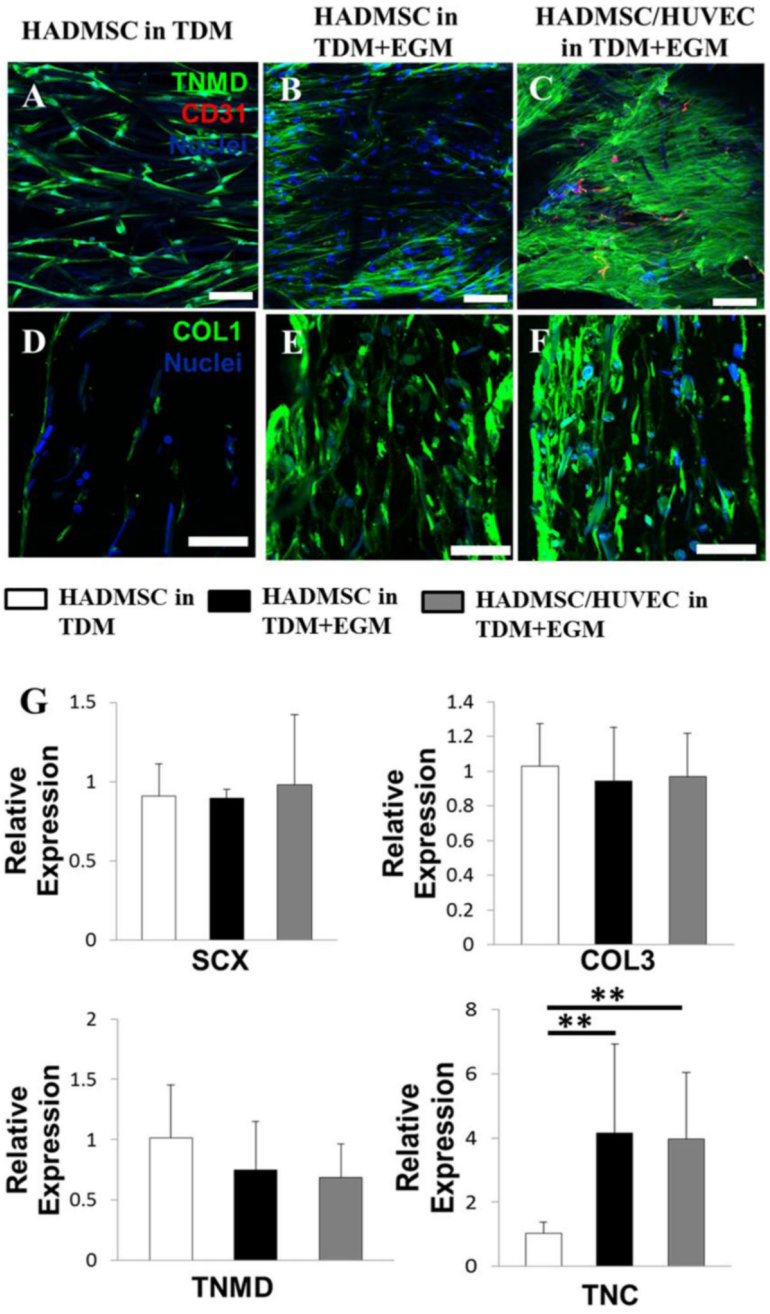

Figure 6.

Co-culture of HADMSC and HUVEC on aligned PLLA fibrous scaffolds promoted tenogenic differentiation in vitro. Representative immunofluorescent staining for TNMD (green), CD31 (red) and nuclei (blue) on aligned PLLA fibrous scaffolds after 21-day culture: (A) HADMSC in TDM, (B) HADMSC in TDM+EGM, (C) HADMSC+HUVEC in TDM+EGM. Scale bars = 100 μm. Cross-sectional immunofluorescent staining for COL1 (green), and nuclei (blue) on aligned PLLA fibrous scaffolds after 21-day culture: (C) HADMSC in TDM, (D) HADMSC in TDM+EGM, (E) HADMSC+HUVEC in TDM +EGM. Scale bars = 100 μm. (G) qPCR analysis. HADMSC or HADMSC-HUVEC were

seeded and conditioned in TDM only or hybrid media with TDM and EGM for 21 days. Relative gene expression is presented as normalized to 18S and expressed relative to HADMSC-seeded scaffolds in TDM only (n=3; ** $p<0.01$)